Aeroelastic reliability based optimisation of composite plates via dual-space surrogate modeling

Roger Ballester Claret, Nicolò Fabbiane, Christian Fagiano, Cédric Julien, Didier Lucor

International Forum on Aeroelasticity and Structural Dynamics
IFASD 2024
17-21 June 2024, The Hague, The Netherlands

AEROELASTIC RELIABILITY BASED OPTIMISATION OF COMPOSITE PLATES VIA DUAL-SPACE SURROGATE MODELING

Roger Ballester Claret[1], Nicolò Fabbiane[1], Christian Fagiano[2], Cédric Julien[2], Didier Lucor[3]

[1]DAAA, ONERA, Institut Polytechnique de Paris
92320 Châtillon, France
roger.ballester_claret@onera.fr
nicolo.fabbiane@onera.fr

[2]DMAS, ONERA, Institut Polytechnique de Paris
92320 Châtillon, France
christian.fagiano@onera.fr
cedric.julien@onera.fr

[3]CNRS, Université Paris-Saclay, Laboratoire Interdisciplinaire des Sciences du Numérique
91400 Orsay, France
didier.lucor@lisn.upsaclay.fr

Keywords: Aeroelasticity, Lamination Parameters, Constrained Optimisation, Efficient Global Optimisation, Reliability-Based Design Optimisation

Abstract: Composite materials are essential in aerospace engineering due to their superior strength-to-weight ratio. This work explores the reliability-based design optimisation of composite plates under aeroelastic constraints with a focus on cost efficiency. We utilise a simplified approach focusing on generating surrogate models through conditioned Gaussian Processes, which predict various aeroelastic responses like flutter speed, gust loads, and static forces. These models help in the effective navigation of the composite design space. We introduce a 5 step optimisation algorithm in which we prioritise minimising the gust response and structure mass while adhering to predefined limits on flutter and strain. The proposed approach not only simplifies the optimisation process but also enhances the understanding and reliability of composite material design in aerospace applications, aiming for improved safety and performance.

1 INTRODUCTION

Aeroelastic phenomena pose significant challenges to the structural integrity and operational efficiency of aircraft wings structures [1], built mostly from composite laminates . This research addresses these challenges by developing a framework for the aeroelastic reliability-based optimisation (RBDO) of composite plates [2], utilising surrogate modeling techniques to optimise design and improve reliability while managing the prohibitive computational costs of direct aeroelastic simulations [3].

The composite plates under study [4] are designed to replicate a two-zone wing structure, with varying ply numbers across the zones to simulate different stiffness and mass distributions [5]. This approach allows for a detailed exploration of aeroelastic effects under realistic operational

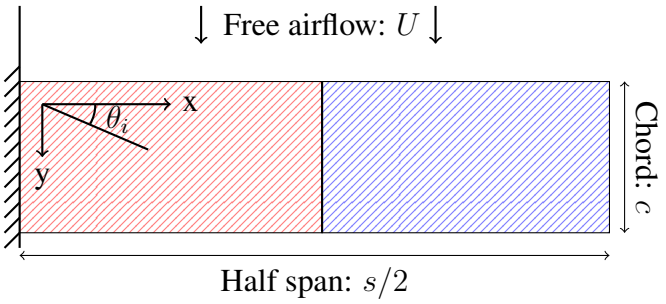

Figure 1: Composite plate immersed in airflow

conditions while maintaining a focus on cost-efficiency. The optimisation process is centered around minimising the mass of the composite structures as well as the gust-induced bending moment at the plate's base [6], a critical factor in aeroelastic assessments, while ensuring that the strain levels and flutter speeds remain within safe operational limits [7].

The optimisation methodology utilised in this study combines Efficient Global Optimisation (EGO) [8] with a constrained optimisation framework. The constraints, maximum allowable strain and a lower bound on flutter speed, are incorporated using the Probability of Feasibility (PoF) approach [9]. This technique modifies the classical Expected Improvement (EI) metric from Bayesian optimisation to factor in the likelihood of constraint satisfaction, thereby guiding the search process towards feasible and optimal solutions .

In the preliminary stages, various Design of Experiments (DoE) configurations are explored based on their spatial properties and the resulting quality of the surrogate models they support [10]. Metrics such as the minimum and maximum-minimum distances between points, along with evaluations of the correlation matrices, are used to select the most effective experimental designs [11].

Given the critical importance of model reliability in RBDO [12, 13], the study rigorously assesses and validates the accuracy of the surrogate models, defined via Kriging (KRG) in the *SMT python* library [14]. This validation is essential to ensure that subsequent optimisations are based on reliable predictions.

Ultimately, the optimisation loop is closed using Genetic Algorithms (GAs) that iteratively refine the design based on surrogate model evaluations [15]. These algorithms permit the reliability based design, adapting the optimisation process to handle complex and discrete variables such as the number of plies or the ply orientation [16].

This paper will detail the methodologies adopted and the results obtained, thereby illustrating the efficacy and robustness of using surrogate models for the aeroelastic reliability-based optimisation of composite plates.

2 COMPOSITE PLATE AND MATERIAL DESCRIPTION

In this study, a rectangular composite plate model is utilised to evaluate aeroelastic behaviours, following principles outlined in the Kirchhoff plate theory combined with the Doublet Lattice Method (DLM) for fluid mechanics representation [17, 18]. This model, which simplifies the plate as being clamped on one edge and free on other edges and submerged into an airflow (Figure 1), is a standard in aeronautics engineering for initial aeroelastic representation.

The plate is constructed of two zones with multiple plies, with each ply oriented at an angle θ_i, potentially including errors as random variables defined by:

$$\theta_i = \bar{\theta}_i + \sigma_{\theta_i} X, \quad X \sim N(0,1), \tag{1}$$

where $\bar{\theta}_i$ and σ_{θ_i} represent the mean and standard deviation of the i-th ply's orientation, respectively.

Table 1: Dimensions and material properties

Parameter	Description	Value	Unit
$s/2$	Half-span	0.3048	m
c	Chord length	0.0762	m
E_{11}	Elastic modulus in 1 direction	140	GPa
E_{22}	Elastic modulus in 2 direction	10	GPa
G_{12}	Shear modulus in 1-2 plane	5	GPa
v_{12}	Major Poisson's ratio	0.3	-
ρ	Density	1600	kg/m^3
t_p	Ply thickness	0.125	mm

2.1 Composite Material Multi-Scale Approach

The optimisation targets finding the best stacking sequence $\boldsymbol{\theta}_{\text{opt}} = [\theta_1, \theta_2, ...]$, with the possible angles being discrete ply angles due to manufacturing constraints [19]. The angles considered for this study are: $0°, \pm 15°, \pm 30°, \pm 45°, \pm 60°, \pm 75°, 90°$. The reduced possibilities and discrete nature end up forming a complex design space characterised by numerous local minima. In order to manage this complex design space, an homogenisation technique is proposed.

2.2 Homogenisation Technique

First of all, the homogenisation method used is based on classical laminate theory [20]. The laminate's behaviour is described using the rigidity matrices A, B, and D, which relate the internal forces and moments to the strains and curvatures experienced by the plate:

$$\begin{pmatrix} N_x \\ N_y \\ N_{xy} \\ \hline M_x \\ M_y \\ M_{xy} \end{pmatrix} = \left[\begin{array}{c|c} A & B \\ \hline B & D \end{array}\right] \begin{pmatrix} \epsilon_x \\ \epsilon_y \\ \gamma_{xy} \\ \hline \kappa_x \\ \kappa_y \\ \kappa_{xy} \end{pmatrix}. \tag{2}$$

The behaviour of our composite stack is determined by 18 variables derived from the A, B, and D matrices, which are influenced by both the stacking sequences and the material properties. Optimising these variables is complex, and can be tedious as in most cases material properties are not subject to change through the optimisation process.

To simplify this complexity, we implement a Lamination Parameter (LP) design approach. This strategy aims to separate the geometric influences from the material's mechanical properties.

We define LPs using the orientations θ of the plies and the total thickness t, as follows:

$$\begin{aligned}
\mathbf{v}^{\mathbf{A}}_{[\mathbf{1},\mathbf{2},\mathbf{3},\mathbf{4}]} &= \frac{1}{t}\sum_{k}^{N}(z_k - z_{k-1})\left[\cos(2\theta_k), \sin(2\theta_k), \cos(4\theta_k), \sin(4\theta_k)\right], \\
\mathbf{v}^{\mathbf{B}}_{[\mathbf{1},\mathbf{2},\mathbf{3},\mathbf{4}]} &= \frac{4}{t^2}\sum_{k}^{N}\frac{(z_k^2 - z_{k-1}^2)}{2}\left[\cos(2\theta_k), \sin(2\theta_k), \cos(4\theta_k), \sin(4\theta_k)\right], \\
\mathbf{v}^{\mathbf{D}}_{[\mathbf{1},\mathbf{2},\mathbf{3},\mathbf{4}]} &= \frac{12}{t^3}\sum_{k}^{N}\frac{(z_k^3 - z_{k-1}^3)}{3}\left[\cos(2\theta_k), \sin(2\theta_k), \cos(4\theta_k), \sin(4\theta_k)\right].
\end{aligned} \tag{3}$$

This redefinition reduces the problem's dimensionality to 12 LPs plus five fixed material dependant variables, thus streamlining the computation of the A, B, and D matrices as per Tsai *et al.* [20]:

$$\mathbf{A} = t\,\tilde{\mathbf{A}}(\mathbf{v}^{\mathbf{A}}), \quad \mathbf{B} = \frac{t^2}{4}\,\tilde{\mathbf{B}}(\mathbf{v}^{\mathbf{B}}), \quad \mathbf{D} = \frac{t^3}{12}\,\tilde{\mathbf{D}}(\mathbf{v}^{\mathbf{D}}). \tag{4}$$

The 12 LPs, symbolised as $\mathbf{v}$, together with the material properties, describe the behaviour of the laminate's matrices A, B, and D. In our study, the total thickness t is also a critical factor, extending our homogenised design space to include 13 variables per zone i of the plate; represented as $(\mathbf{v}, t)_i$.

For the specific scenario of aeroelastic analysis under pure bending conditions, we focus primarily on the D matrix. Moreover we simplify the variable space further to just $(\mathbf{v}_1^D, \mathbf{v}_3^D, t)$ by imposing a $(v_2^D, v_4^D) = (0, 0)$ condition. Finally, considering that the plate only has 2 zones, the final design space is a 6 variable design space such as:

$$(\mathbf{v}, t) = (\mathbf{v}^D_{1\ 1}, \mathbf{v}^D_{3\ 1}, \mathbf{v}^D_{1\ 2}, \mathbf{v}^D_{3\ 2}, t_1, t_2). \tag{5}$$

This approach effectively transforms the detailed multi zone ply orientation sequence $\boldsymbol{\theta}$ into a more manageable set of homogenised variables, encapsulating the essential design features into a simplified model.

3 AEROELASTIC RESPONSE

Aeroelasticity is crucial for ensuring the structural integrity and performance of aircraft components under aerodynamic forces. This study refines the understanding of aeroelastic behaviour in composite wing structures through a simplified plate model analysed using the Doublet Lattice Method (DLM) with *MSC NASTRAN* software for comprehensive aeroelastic simulations [17, 18].

3.1 Static Aeroelastic Analysis

Static aeroelastic analysis assesses the plate's ability to maintain structural integrity under normal operating loads. This involves examining how the composite structure manages to sustain and revert to its original shape against aerodynamic forces. The concept of static aeroelastic stability, which forms an equilibrium between structural and aerodynamic forces, is fundamental here and described by the equation:

$$\mathbf{K}\mathbf{q} = \mathbf{F}_a(\mathbf{q}, \rho, U) \tag{6}$$

where $\mathbf{K}$ represents the stiffness matrix of the plate, $\mathbf{q}$ is the generalised displacement vector, and $\mathbf{F}_a$ denotes the aerodynamic force vector dependent on the wing's deformed geometry, air density (ρ), and flight speed (U) [7].

3.2 Flutter Analysis

Flutter, an instability coming from aerodynamic, elastic, and inertial force interactions, poses significant risks to flight safety. Determining the flutter boundary, marked by the critical flutter speed, is essential for predicting and mitigating this instability. The flutter analysis uses both time and frequency domain approaches:

$$\mathbf{M}\ddot{\mathbf{q}} + \mathbf{K}\mathbf{q} = \mathbf{F}_a(\mathbf{q}, \dot{\mathbf{q}}; \rho, U), \tag{7}$$

where M is the mass matrix. In the frequency domain, the equations become:

$$(\mathbf{K} + \rho U^2 \mathbf{K}_a(\omega) - \lambda^2 \mathbf{M})\hat{\mathbf{q}} + i\lambda\rho U \mathbf{C}_a(\omega)\hat{\mathbf{q}} = \mathbf{0}, \tag{8}$$

$$\lambda = \sigma + i\omega, \tag{9}$$

identifying λ as the complex eigenvalue indicating growth rate (σ) and frequency (ω), with $\mathbf{K}_a$ and $\mathbf{C}_a$ as the aerodynamic stiffness and damping matrices, respectively [21].

3.2.1 Hump Modes in Flutter Analysis

In the context of flutter analysis, hump modes are characterised by maxima in the flutter speed versus frequency curves [22, 23]. These modes are particularly critical as they can represent conditions under which the structure is highly susceptible to flutter instabilities at specific frequencies. The analytical detection of hump modes involves examining the frequency response of the system and identifying where these local maxima occur. Within figures 2, a hump mode can be observed in mode 3, where the growth rate (σ) is plotted against the wind velocity . By slightly modifying the material properties of the structure we can observe how the mode turns unstable as $\sigma > 0$ when $V_{flutter} = 153m/s$.

3.3 Wind Gust Response Analysis

There is an existing need to understand the structural response to wind gusts, as gusts can impose sudden, severe stresses to aircraft structures. The gust response of those structures is modeled through transient analysis reflecting the time-varying nature of aerodynamic forces:

$$\mathbf{M}\ddot{\mathbf{q}} + \mathbf{C}\dot{\mathbf{q}} + \mathbf{K}\mathbf{q} = \mathbf{F}_a(\mathbf{q}; \rho, U) + \mathbf{F}_{gust}(t), \tag{10}$$

with $\mathbf{F}_{gust}(t)$ as the gust force impacting over time, added to the regular aerodynamic forces [6, 18]. This analysis is vital for preparing the aircraft to withstand and adapt to rapid changes in the aerodynamic environment, thereby enhancing its resilience and operational safety.

4 METHODOLOGY

4.1 Formulation of the Probabilistic Optimisation Problem

Our goal in optimising composite wing structures is to minimise both the expected gust response and the overall mass, taking into account uncertainties inherent in composite ply fabrication. These uncertainties can significantly impact the aeroelastic response and structural integrity.

Objective Function: We aim to determine the optimal stacking sequences $\boldsymbol{\theta}_i = [\theta_1, \theta_2, \ldots, \theta_N]_i$ that minimises the expected value of the gust-induced maximum bending moment, denoted by

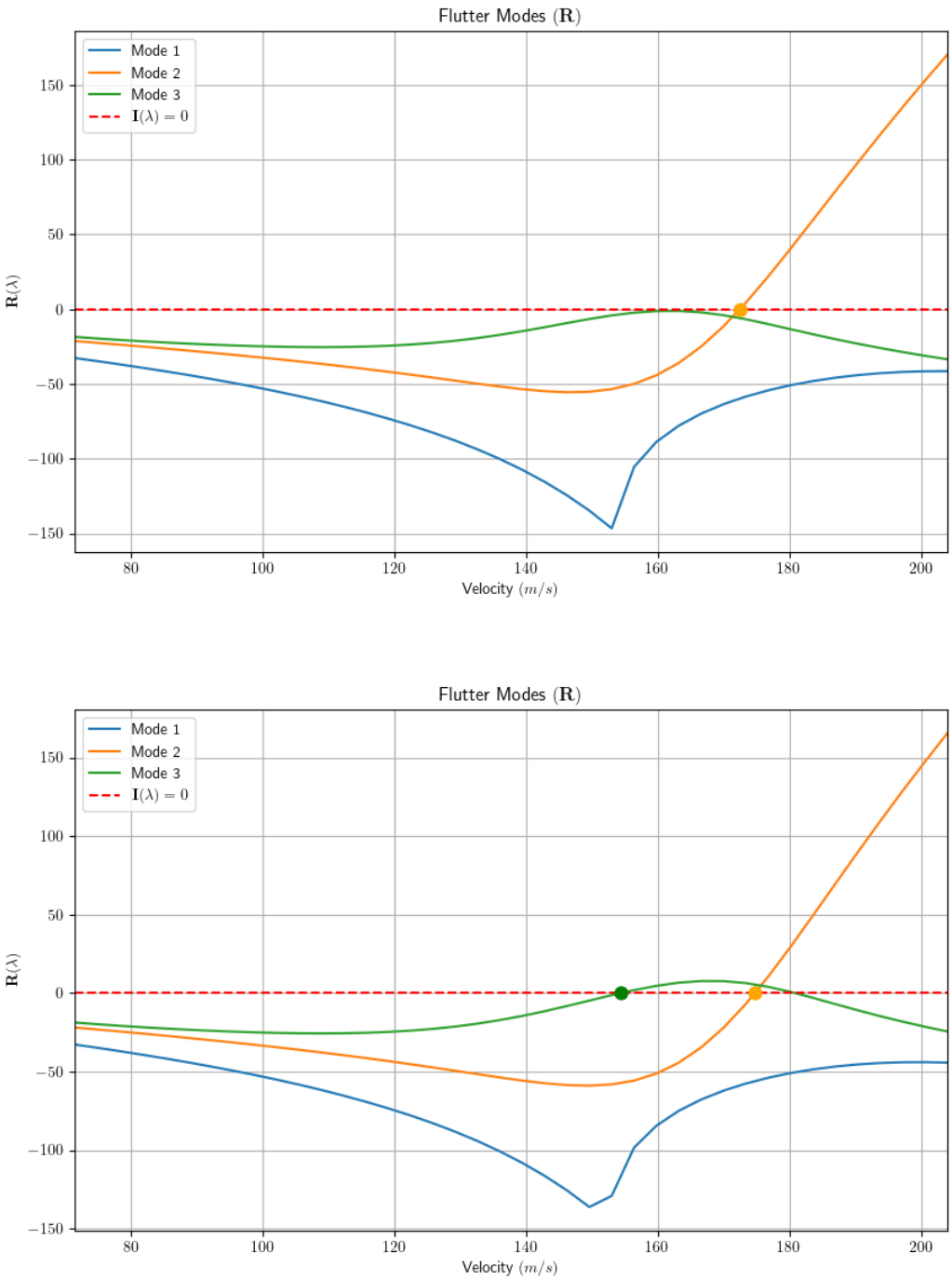

Figure 2: Hump mode representation in mode 3.

M_x, while also minimising the thickness (mass) $(t_1 + t_2)$ which is directly linked to the number of plies $\mathbf{N} = (N_1, N_2)$. The optimisation function, framed within a probabilistic context, is expressed as:

$$\mathbb{E}[f(\boldsymbol{\theta})] = (t_1 + t_2) + w_{\text{gust}} \cdot \mathbb{E}[M_x(\boldsymbol{\theta})], \tag{11}$$

where $\mathbb{E}[\cdot]$ represents the expected value, accounting for variability in the input ply angles $\boldsymbol{\theta} \sim \mathcal{N}(\bar{\boldsymbol{\theta}}, \Sigma)$ and $\mathbf{N}$, the dimension of $\boldsymbol{\theta}$. The coefficient w_{gust} is a weighting factor emphasising the importance of the gust effect.

Constraints: The design must adhere to probabilistic constraints that ensure critical performance thresholds are not exceeded:

1. **Flutter Speed Constraint:** The probability that the flutter speed falls below a critical threshold must be minimised for aeroelastic stability:

$$\mathbb{P}(V_{\text{flutter}}(\boldsymbol{\theta}) < V_{\text{min}}) \leq \mathbb{P}^{V}_{\text{limit}}, \tag{12}$$

2. **Maximum Equivalent Strain Constraint:** The probability that the equivalent strain exceeds a maximum allowable level must be controlled to prevent structural failure:

$$\mathbb{P}(\epsilon_{\text{equivalent}}(\boldsymbol{\theta}) > \epsilon_{\text{max}}) \leq \mathbb{P}^{\epsilon}_{\text{limit}}, \tag{13}$$

Here, $\mathbb{P}(\cdot)$ denotes the probability of the event, which is maintained below predefined limits $\mathbb{P}^{\cdot}_{\text{limit}}$ set based on safety and performance standards.

Probabilistic Optimisation Problem: The optimisation problem, now formulated in probabilistic terms, seeks a design that not only minimises the expected objective function but also adheres strictly to the constraints with high probability:

$$\begin{aligned} \underset{(\bar{\boldsymbol{\theta}})}{\text{minimise}} \quad & \mathbb{E}[f(\boldsymbol{\theta})] \\ \text{subject to} \quad & \mathbb{P}(V_{\text{flutter}}(\boldsymbol{\theta}) < V_{\text{min}}) \leq \mathbb{P}^{V}_{\text{limit}}, \\ & \mathbb{P}(\epsilon_{\text{equivalent}}(\boldsymbol{\theta}) > \epsilon_{\text{max}}) \leq \mathbb{P}^{\epsilon}_{\text{limit}}. \end{aligned} \tag{14}$$

4.2 Methodology layout

Below is an overview of the workflow used in our methodology and the individual description of each step.

4.3 Step 1: Design of Experiments (DoE)

The first step elaborates on the Design of Experiments (DoE) methodologies considered in this study, including techniques like Quasi Monte Carlo and Latin Hypercube Sampling. Furthermore, it details the metrics used to evaluate the quality of these experimental designs.

4.3.1 DoE Techniques Initially Considered

- **Latin Hypercube Sampling (LHS)**: A stratified sampling technique that partitions the range of each variable into N non-overlapping intervals of equal probability and randomly samples from each interval, ensuring all portions of the distribution are represented.
- **Quasi Monte Carlo (QMC)**: Uses low-discrepancy sequences to cover the design space more uniformly than regular Monte Carlo. The Sobol sequence is employed to determine the indexes.
- **Regular Monte Carlo**: Randomly selects points in the design space with uniform probability. It lacks the structured approach of other methods but is simple and robust.

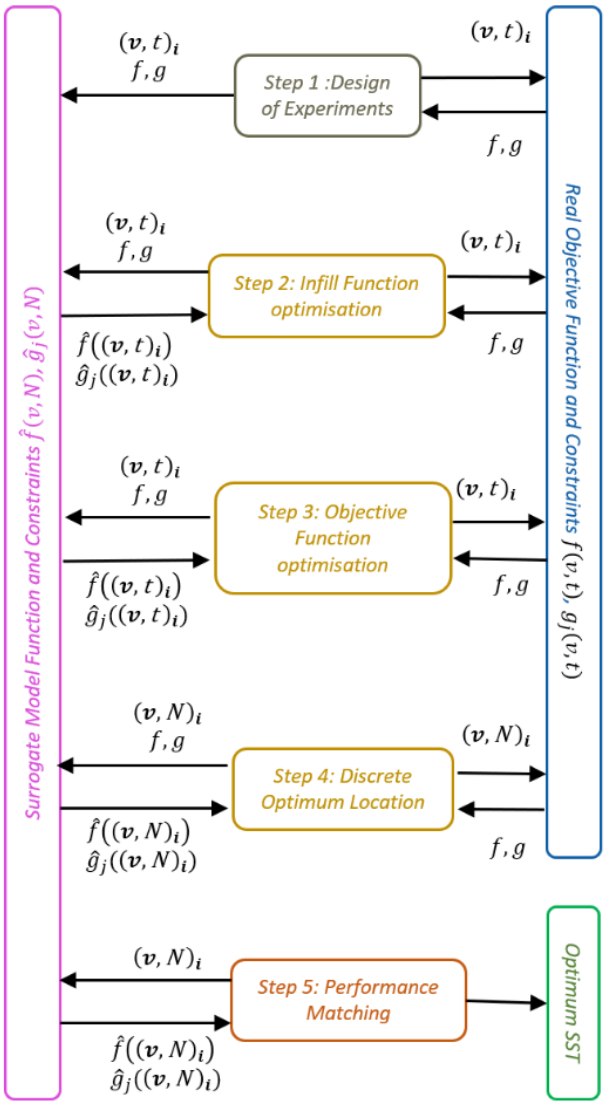

Figure 3: Workflow of the optimisation methodology.

4.3.2 Experiment Quality Metrics

Quality of the designs of experiments was assessed using several metrics to ensure data reliability and effectiveness of the design:

- **Minimum Distance (MinDist)**: Ensures experiments are not clustered; calculated as:

$$\text{MinDist} = \min_{i \neq j} \|\mathbf{x}_i - \mathbf{x}_j\|. \tag{15}$$

- **MaxMin Distance**: Aims to maximise the smallest distance between points:

$$\text{MaxMinDist} = \max_{\mathbf{x} \in \mathcal{X}} \min_{i \neq j} \|\mathbf{x} - \mathbf{x}_i\|. \tag{16}$$

- **Correlation Matrix Evaluation**: Low correlations indicate more distinct experimental outcomes; it assesses the independence of factorial levels.

4.4 Step 2: Infill Function Optimisation

Following the initial DoE, the methodology employs Efficient Global Optimisation (EGO) to enhance the quality of the surrogate model, notably near the optimum solution. The EGO algorithm iteratively adds points to the surrogate models by optimising an acquisition function, which helps to identifying new, informative data points. This process is used to refine the surrogate model's predictions over successive iterations. The surrogate models are dynamically updated as new data points are incorporated, with the continuous integration of new data points leading to a progressive improvement in the model's accuracy. The acquisition function used in this case is a modification of the classic EI to treat constrained optimisation [9]. The optimisation of the acquisition function is solved via differential evolution algorithms.

4.4.1 Expected Improvement

The standard form of EI [8] is defined as the expected increase in objective function value over the current best observation $f(\mathbf{v}^*, t^*)$, and is given by:

$$EI(\mathbf{v}, t) = \mathbb{E}[\max(\hat{f}(\mathbf{v}^*, t^*) - \hat{f}(\mathbf{v}, t), 0)]. \tag{17}$$

Assuming a Gaussian Process model for the objective function with mean $\mu(\mathbf{v}, t)$ and standard deviation $\sigma(\mathbf{v}, t)$, the EI at any point $(\mathbf{v}, t)$ in the design space can be expanded using the properties of the normal distribution as follows:

$$\begin{aligned} EI(\mathbf{v}, t) = (\hat{f}(\mathbf{v}^*, t^*) - \mu(\mathbf{v}, t))\Phi\left(Z(\mathbf{v}, t)\right) \\ + \sigma(\mathbf{v}, t)\phi\left(Z(\mathbf{v}, t)\right), \end{aligned} \tag{18}$$

where $Z(\mathbf{v}, t)$ is the improvement potential standardised,

$$Z(\mathbf{v}, t) = \frac{\hat{f}(\mathbf{v}^*, t^*) - \mu(\hat{f}(\mathbf{v}, t))}{\sigma(\hat{f}(\mathbf{v}, t))}, \tag{19}$$

and Φ and ϕ are the cumulative and probability density functions of the standard normal distribution, respectively.

4.4.2 Expected Improvement with Constraints

The PoF is used to assess the likelihood that a given design point $(\mathbf{v}, t)$ adheres to the constraints and is modeled using Gaussian Processes for each constraint:

$$PoF(\mathbf{v}, t) = \Phi\left(-\frac{\mu_c(\mathbf{v}, t)}{\sigma_c(\mathbf{v}, t)}\right). \tag{20}$$

The optimisation process involves iteratively selecting design points that maximise the product of EI and PoF, effectively balancing the exploration of the design space with adherence to the constraints.

$$(\mathbf{v}_{\text{next}}, t_{\text{next}}) = \arg\max_{(\mathbf{v},t)}(EI(\mathbf{v}, t) \times PoF(\mathbf{v}, t)). \tag{21}$$

This methodology, from initial surrogate model development through constrained optimisation, ensures optimum surrogate construction and design space exploration under varying aeroelastic conditions.

4.5 Step 3: Objective Function Optimisation

The third step involves optimising the objective function within the surrogate model to find a deterministic solution in the continuous design space $(\mathbf{v}, t)$. This optimisation identifies the best possible configuration for:

$$\min_{\mathbf{v},\mathbf{t}_i} \hat{f}(\mathbf{v}, t). \tag{22}$$

The transformation involves replacing the probabilistic measures with deterministic values that represent a conservative estimate of the constraint. For instance, in the case of the flutter speed constraint, the probability that the flutter speed falls below a critical threshold is transformed into a deterministic constraint as:

$$V_{\text{flutter}}(\mathbf{v}, t) \geq V_{\text{min}}. \tag{23}$$

Similarly, for the maximum equivalent strain constraint:

$$\epsilon_{\text{eq}}(\mathbf{v}, t) \leq \epsilon_{\text{max}}. \tag{24}$$

Once the deterministic constraints are established, an iterative optimisation procedure is employed to find the optimal design point. Typically, this involves computing the objective function and constraints at the current design point via the NASTRAN model, then adding this point to the design space and recomputing the surrogate model. This process continues iteratively until convergence is achieved, meaning that the optimal design point remains stable across iterations and satisfies all constraints within acceptable tolerances.

4.6 Step 4: Discrete Optimum Location

After determining the continuous optimal values for the thickness of the two sections of the composite plate t, the next step is to translate these values into practical, discrete integers that can be used in manufacturing $(t_1, t_2) \rightarrow (N_1, N_2)$. The number of plies in any section of a composite structure must be a whole number; hence, the challenge lies in converting continuous solutions from the optimisation model into viable discrete configurations.

Optimisation Transition to Discrete Values: The optimisation problem under consideration ensures that the structural and operational constraints are still respected in the discrete domain:

$$\begin{aligned} \min_{(\mathbf{v},\mathbf{N}_i)} & f(\mathbf{v}, N), \\ V_{\text{flutter}}(\mathbf{v}, N) &\geq V_{\min}, \\ \epsilon_{\text{eq}}(\mathbf{v}, N) &\leq \epsilon_{\max}. \end{aligned} \tag{25}$$

Here, $\mathbf{N}$ denotes the set of integer values (N_1, N_2) for the number of plies required in each section.

To select the optimum discrete values for the number of plies (N_1, N_2), the approach is to round the continuous values $(t_1^*/t_p, t_2^*/t_p)$ to the nearest integers, with t_p being the thickness of the base layer. However, simply rounding each value may lead to solutions which do not satisfy the aeroelastic constraints, so compliance conditions are introduced:

Ensuring Constraint compliance: We apply the following criteria to determine the best rounding approach:

- In order to comply with the symmetry condition the thickness of each region must be a multiple of $2t_{ply}$
- The sum of the discrete values $\sum N_i$ has to exceed the sum of the optimised continuous values $\sum(t_i^*/t_p)$. This ensures that the new configurations have the same or higher compliance of the constraints.
- Among the feasible rounding options, the choice that minimises the total deviation from the continuous optimal values is preferred, as this typically maintains closer adherence to the predicted performance and cost metrics.

The final configuration of N will be denoted as N_{opt}. This step ensures that the theoretically optimal design is translatable into a practically manufacturable product while adhering to the constraints of discrete manufacturing processes.

4.7 Step 5:Performance Matching for Reliability-Based Design Optimisation (RBDO)

The final step involves using the surrogate model to run a RBDO solver based on GAs [15, 24]. This stage aims to find the final stacking sequence that meets the reliability requirements under operational conditions. This phase considers both the performance metrics and the reliability of the material system, finalising the design process and yielding the final stacking sequence $\boldsymbol{\theta}$.

The RBDO process commences within a precisely defined design space where the number of plies, denoted as $\mathbf{N}_{opt}$, is fixed based on the optimal solution derived from earlier deterministic optimisation stages. Therefore the reliability based optimisation problem can be rewritten as:

$$\begin{aligned} \underset{(\mathbf{v})}{\text{minimise}} \quad & \mathbb{E}[\hat{M}_x(\mathbf{v}(\boldsymbol{\theta}))] \\ \text{subject to} \quad & \mathbb{P}(\hat{V}_{\text{flutter}}(\mathbf{v}(\boldsymbol{\theta})) < V_{\text{min}}) \leq \mathbb{P}^{V}_{\text{limit}}, \\ & \mathbb{P}(\hat{\epsilon}_{\text{eq}}(\mathbf{v}(\boldsymbol{\theta})) > \epsilon_{\text{max}}) \leq \mathbb{P}^{\epsilon}_{\text{limit}}, \end{aligned} \tag{26}$$

with the $\hat{M}_x$, $\hat{V}_{\text{flutter}}$ and $\hat{\epsilon}_{\text{eq}}$ representing the surrogate model response for a certain input $(\mathbf{v}, \mathbf{N}_{opt})$ and the LPs being a function of the stacking sequence $\mathbf{v}(\boldsymbol{\theta})$.

4.7.1 Implementation of GAs in RBDO

GAs are employed for solving the RBDO due to their robustness in handling complex, non-linear optimisation problems with multiple local minima. GAs simulate processes in natural evolution, such as selection, crossover, and mutation, to iteratively improve solution quality:

- **Initialisation**: Begin with a randomly generated population of potential solutions based on the defined number of plies $\mathbf{N}_{opt}$.
- **Fitness Evaluation**: Each individual in the population is evaluated using a fitness function that incorporates both the objective function and constraints of the RBDO. This function typically reflects the structural performance and reliability criteria under variable material properties and manufacturing conditions.
- **Selection**: Select individuals based on their fitness scores to form a mating pool; methods such as tournament selection or roulette wheel selection are commonly used.
- **Crossover and Mutation**: Generate new individuals (offspring) by combining and modifying the genetic information (ply orientation and ply drops) of selected parents to introduce diversity and explore new areas of the design space.
- **Replacement**: Replace less fit individuals with new, potentially superior offspring to form a new generation.

4.7.2 Handling Variability in Material Properties

One of the primary challenges in RBDO is the variability issued by the manufacturing inaccuracies, which significantly impact the performance and reliability of the designed component. The GA incorporates this variability by evaluating via a Monte Carlo algorithm the fitness of each design under different realisations of the induced error σ_{θ_i}, effectively simulating the performance across a range of probable manufacturing outcomes. This approach ensures that the optimised design is not only optimal for the nominal scenario but also robust and reliable against angular variations in the stacking sequence.

4.7.3 Optimisation Criteria and Algorithm Termination

The optimisation continues until a satisfactory level of fitness is achieved or a predetermined number of generations is reached. The termination criteria directly influence the computational cost and quality of the solution. Typically, the process iterates until the improvement between generations falls below a minimal threshold, indicating that further exploration may yield diminishing returns. Moreover, the GA is run several times in order to account for the stochastic nature of this optimisation model.

5 RESULTS

This section presents the results for the five steps of our methodology: 1. Design of Experiments, 2. Infill Function Optimisation, 3. Objective Function Optimisation, 4. Discrete Opti-

mum Location and 5. Performance Matching for Reliability-Based Design Optimisation.

5.1 Step 1: Design of Experiments

In our investigation, three different DoE methods were employed to assess their effectiveness in exploring the design space of the problem at hand $(\mathbf{v}^D_{1\ 1}, \mathbf{v}^D_{3\ 2}, \mathbf{v}^D_{1\ 2}, \mathbf{v}^D_{3\ 1}, t_1, t_2)$: MC, LHS and QMC. For the first two methods, given their Bayesian behaviour, 1000 different DoEs were generated, and the best-performing design was selected based on the criteria of minimal distance between points, the quality index and the maximin criterion value.

Table 2: Comparison of DoE Methods

Method	Metric	Value
Monte Carlo (MC)	MinDist	0.452
	Quality Index	0.161
	Maximin Criterion Value	1.806
Latin Hypercube Sampling (LHS)	MinDist	0.483
	Quality Index	0.152
	Maximin Criterion Value	1.818
Quasi Monte Carlo (QMC)	MinDist	0.449
	Quality Index	0.119
	Maximin Criterion Value	1.861

The analysis of the DoEs outcomes clearly demonstrates that the QMC method outperformed both LHS and MC. Specifically, QMC achieved the best balance of minimum distance between points, lowest quality index, and highest maximin criterion value. The minimal distance, which ensures that points are not overly clustered, is slightly smaller in the QMC though with values very near the ones offered by MC and LH. The quality index, being the lowest for QMC, indicates a higher overall quality of the experiment design, suggesting that this method can better manage the variance within the sampling process. Furthermore, the maximin criterion value being highest for QMC highlights its capability to maximise the smallest distance between any two points, thus ensuring a better spread across the design space.

Given these results, the DoE generated via QMC method was selected for use in the optimisation process. The QMC method's ability to systematically cover the design space while maintaining low variability in point distribution makes it particularly suitable for constructing accurate and reliable surrogate models. This choice is expected to significantly enhance the fidelity of our optimisation framework, ensuring that the surrogate models developed are both precise and robust.

5.2 Step 2: Infill Function Optimisation

The surrogate model was iteratively refined using the EGO algorithm previously introduced, focusing on improving the $EI * PoF$ metric. This method allowed us to identify potential design points that efficiently balanced between exploration and exploitation of the design space.

The progression of the $EI * PoF$ metric, initially showing substantial improvement, demonstrates a declining trend in later iterations, suggesting that the search is nearing optimal regions within the explored design space. Simultaneously, the quality of the correlation matrix, which assesses the surrogate model's accuracy, exhibits a worsening trend as iterations progress given that adding new points disturbs the equilibrated initial distribution. Despite the fluctuating per-

formance, the $EI * PoF$ metric remained above critical thresholds, ensuring that the design points never heavily distorted the overall quality of the surrogate models.

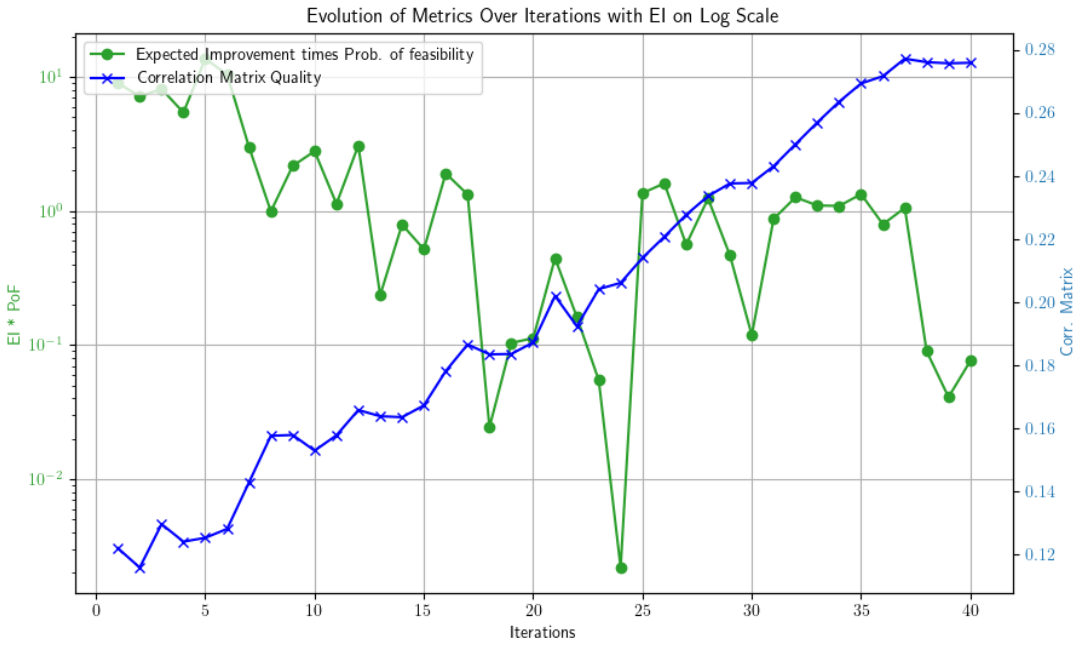

Figure 4: Evolution of Metrics Over Iterations with $EI * PoF$ on Log Scale.

5.3 Step 3: Objective Function Optimisation

The optimisation phase of our study successfully identified optimal design parameters that balance the aeroelastic performance with material efficiency. Through the application of the surrogate model within a deterministic framework, we achieved a design configuration that minimised the bending moment while adhering to flutter speed and maximum strain constraints set by the predetermined limits.

Optimisation Results:

- **Design Parameters:** The optimal lamination parameters were determined to be:

$$(\mathbf{v}_{1\ 1}^{D}, \mathbf{v}_{3\ 1}^{D}, \mathbf{v}_{1\ 2}^{D}, \mathbf{v}_{3\ 2}^{D}, t_1, t_2) = (-0.4313, -0.4901, -0.3992, -0.5180, 2.1468, 1.4062).$$

- **Bending Moment:** The resulting design configuration yields a bending moment of only $202.102Nm$, indicating a significant improvement in structural response under loading conditions.
- **Flutter Speed and Maximum Strain:** Both the flutter speed and maximum strain values found were the limit values (corresponding to $\epsilon_{max} = 0.003$ and $V_{min} = 171.5m/s$), illustrating the model's capability to adhere to critical performance thresholds with both constraints being activated at the same time.

Surrogate Model Predictions:

- The standard deviations from the surrogate model predictions provide insights into the model's accuracy and reliability:

- **Strain:** The standard deviation for strain predictions was measured at 7.147×10^{-6}, reflecting high precision in strain estimation under operational conditions.
- **Flutter Speed:** A standard deviation of $0.0496 m/s$ for flutter speed underscores the model's effectiveness in capturing dynamic aeroelastic behaviours.
- **Gust-induced Bending Moment (Mx):** The standard deviation for the gust-induced bending moment was $0.0828 Nm$, demonstrating the model's response prediction capabilities.

Upon adding the initially identified optimum points to the surrogate model and re-computing it, a subsequent optimisation run identified a new point. The parameters for this new optimal configuration were found at

$$(\mathbf{v}^D_{1\ 1}, \mathbf{v}^D_{3\ 1}, \mathbf{v}^D_{1\ 2}, \mathbf{v}^D_{3\ 2}, t_1, t_2) = (-0.4717, -0.5191, -0.3894, -0.6965, 2.1352, 1.4136).$$

Being only 0.1483 units away from the previous optimum, indicating a minimal shift in the design space. The bending moment generated by gust in the new point is $197.596 Nm$, only slightly improving the last computed point.

Due to the proximity in design space and potential distortion effects on the surrogate model's quality, this new point was not added to the model database. The decision was based on the desire to maintain the integrity and reliability of the surrogate model without introducing significant noise or bias from closely spaced data points.

Analysis of Strain Distribution in Optimum result: The optimisation process involved evaluating the strain distribution across the composite plate to ensure that the design adheres to structural integrity standards under operational loads. The resulting strain map, illustrated in Figure 5, provides a detailed visualisation of the equivalent strain across the plate.

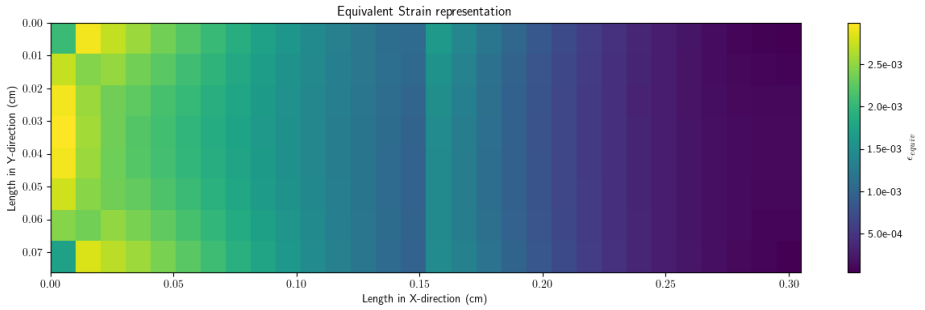

Figure 5: Equivalent strain distribution across the plate, highlighting the multi-zone behaviour with varying strain intensities.

The strain map clearly shows the multi-zone behaviour of the plate, with varying strain intensities evident across different sections. This behaviour shows how different areas of the plate will respond under specific loading conditions, which is fundamental in tailoring the material properties and thickness to meet specific design requirements.

Flutter Analysis Visualisation for optimal result: The close proximity to a hump mode in the flutter analysis is depicted in the figure below, indicating the critical nature of the design in terms of aeroelastic stability, which will have a major role in the RBDO.

This step underscores the efficiency of the surrogate model in navigating the complex design

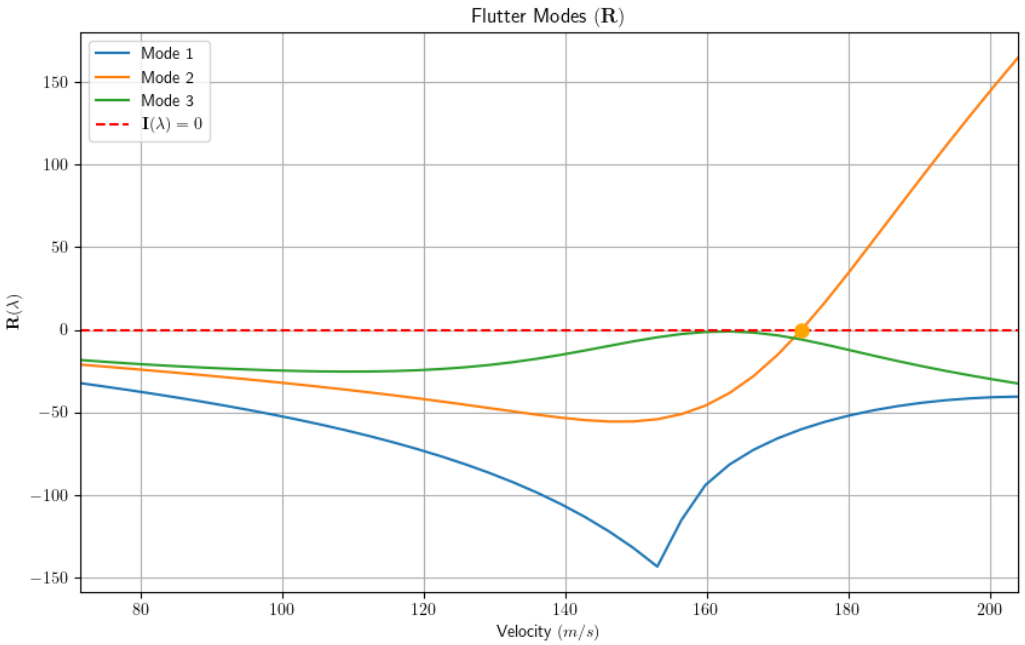

Figure 6: Visualisation of the eigenvalue analysis showing the proximity to a hump mode in the flutter analysis, illustrating the critical interaction between aerodynamic and structural dynamics at the optimised design point.

space of aeroelastic structures, achieving an optimised design that not only meets but effectively balances between performance objectives and computational cost.

5.4 Step 4: Discrete Optimum Location

Following the successful identification of the optimal solutions for the lamination parameters in the continuous design space, the next phase involved transitioning these solutions to practical, discrete variables alignable with actual manufacturable composite plies. This transition is of paramount importance to ensure that the design solutions are not only theoretically optimal but also viable for real-world production.

Conversion to Discrete Variables: The optimisation sought to determine the nearest feasible stacking sequence configurations that would conform to manufacturable standards. Given the continuous optimal results: $(t_1, t_2)_{opt} = (2.1352, 1.41360567625)$ if we divide by the ply thickness t_p we obtain $(t_1/t_p, t_2/t_p)_{opt} = (17.0823, 11.3088)$. Therefore, the the number of plies will be $(N_1, N_2) = (18, 12)$.

The optimisation via differential evolution was now launched with the fixed values of $(N_1, N_2) = (18, 12)$. With the new computed points being added to the surrogate in order to refine it, after a total of 3 iterations the optimum response obtained was:

Adjusted Optimal Bending Moment: The bending moment for this configuration was calculated to be $182.45Nm$, which was the lowest among the considered configurations. **Constraints:** Both the flutter speed and maximum strain values found were the limit values (corresponding to $\epsilon_{max} = 0.003$ and $V_{min} = 171.5m/s$),

This point was not further added to the surrogate models in order to enhance the quality of the

response in the $(N_1, N_2) = (18, 12)$ design zone given the low variability and small distance to the previously computed points.

5.5 Step 5: Performance Matching for RBDO

This phase focused on minimizing gust response, constrained by flutter speed and strain parameters, with a fixed value of $(N_1, N_2) = (18, 12)$. The RBDO employed a GA, rigorously designed to handle the inherent uncertainties in the ply orientation given by the fabrication processes.

To ensure the effectiveness and efficiency of the GA, it is imperative to fine-tune its parameters and operational conditions. The fine-tuning process involved iterative testing and validation against a set of benchmark problems, with adjustments made based on the performance metrics such as convergence rate and solution quality. Parameters such as population size, mutation rate, and crossover probability were adjusted in small increments, while monitoring the impact on the GA's ability to find optimal solutions within a reasonable timeframe. This iterative approach allowed us to identify the optimal settings that balance exploration and exploitation within the GA framework.

Table 3: Conditions and Parameters of the GA

Parameter	Value
Population Size	1000
Crossover Probability	0.8
Mutation Probability	0.3
Elitism group	100
Convergence Criterion	100 Generations
Standard Deviation σ_θ	2°
Monte Carlo Samples	50000

Table 3 summarizes the key settings and values used in the GA, which were fine-tuned as described. All of these parameters were previously defined. Additionally, the table includes the standard deviation σ_θ, representing the variability introduced in the composite materials ply orientation, and the number of samples used in the Monte Carlo analysis.

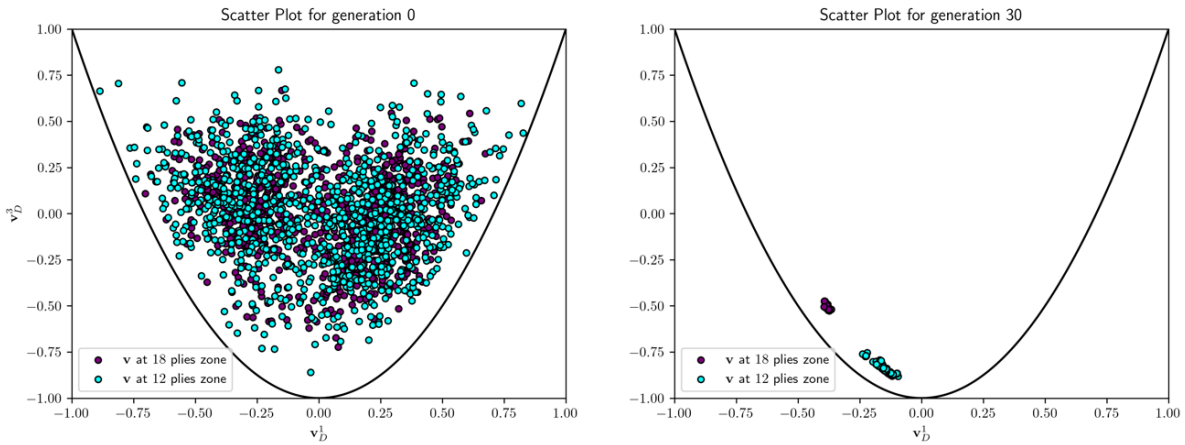

Figure 7: Visualisation of the design space exploration by the GA for the 1st and 30th generations.

Figure 7 illustrates the exploration of the $(\mathbf{v}_1^D, \mathbf{v}_3^D)$ design space during two distinct generations of a GA run, specifically the 1st and the 20th. The plot emphasizes the broad initial exploration,

and the distribution of solutions within the 20th generation, concentrating the points close to the optimal solutions of $(\mathbf{v}_1^D, \mathbf{v}_3^D)$ for each region of the plate. These images demonstrate the GA's ability to explore the design space effectively and to increasingly focus on regions surrounding the fittest individuals as generations progress.

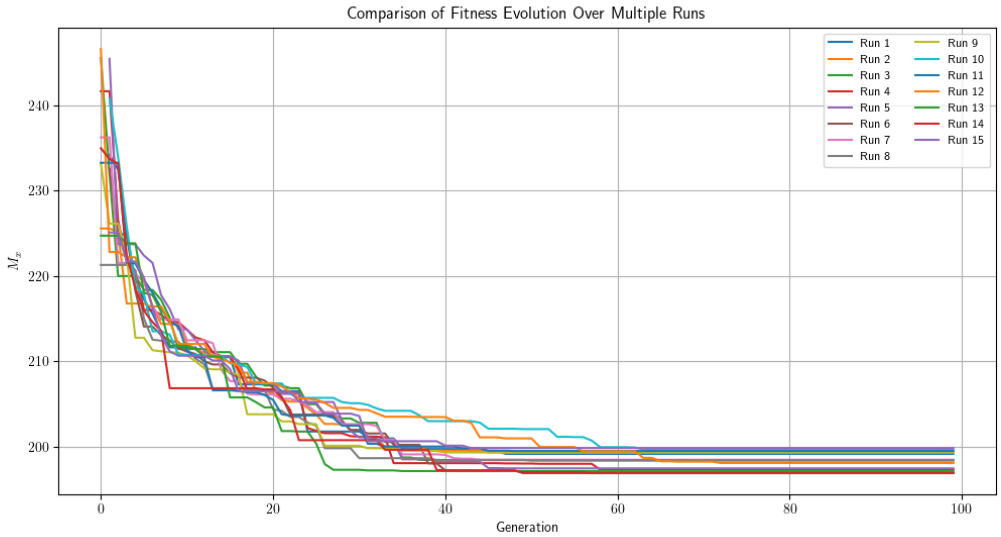

Figure 8: Convergence plot of the gust response obtained with GA through the RBDO process, showing the optimisation progression over 100 generations. Consistency across fifteen separate runs with different initial conditions underlines the algorithm robustness.

Moreover, the convergence of the GA is evaluated to study the reliability and efficiency of the optimisation. Figure 8 displays the convergence plot of the algorithm, showing the optimisation's evolution across 20 generations. This plot includes results from five distinct runs of the algorithm, providing a comprehensive review of its convergence behavior. The consistency observed across these runs underscores the algorithm's robustness and reliability in identifying an optimal solution, with all runs converging by a maximum of 15 iterations. Within Figure 8, the value for the fittest individual that meets all probabilistic constraints is depicted.

6 CONCLUSION

This study has successfully demonstrated the application of aeroelastic Reliability-Based Design Optimisation (RBDO) for composite plates utilising dual-space strategy together with surrogate modeling. Our approach has systematically addressed the multifaceted challenges of designing aerospace composite structures, where both performance optimisation and reliability assurance are critical. The five-step methodology, integrating sophisticated statistical and computational techniques, has yielded a robust and reliable design, optimised for both aeroelastic performance and manufacturability.

The first step, involving an extensive Design of Experiments (DoE), established a strong foundation for the subsequent modeling efforts. By employing a Quasi Monte Carlo (QMC) algorithm we ensured comprehensive coverage of the design space, which allows for accuracy and reliability of the surrogate models. The spatial distribution metrics from this phase indicated excellent design space exploration, setting the stage for effective surrogate model development.

In the second step, infill function optimisation, we refined the surrogate models through Efficient Global Optimisation (EGO), focusing on the Expected Improvement metric constrained

by the Probability of Feasibility. This step helped enhance the model's predictive accuracy, thereby enabling more precise identification of the optimal design points. The optimisation of the infill function significantly improved the convergence of the model, demonstrating the strength of integrating EGO with a probabilistic constraint handling.

The third step, objective function optimisation, utilised the enhanced surrogate models to optimise the objective function within a continuous design space. The results from this phase were revealed a substantial reduction in the expected gust-induced bending moment and the overall structural weight, thereby confirming the efficacy of our surrogate-based optimisation approach.

Transitioning to the fourth step, discrete optimum location, we adjusted the continuous solutions to accommodate the discrete nature of manufacturing constraints related to ply thickness. This step ensured that the theoretical optimisations were feasible in practical manufacturing scenarios, highlighting the importance of considering discrete variables in composite structure design.

Finally, the fifth step involved performance matching and RBDO using Genetic Algorithms. This phase was geared towards ensuring that the final design adhered to stringent reliability thresholds under operational uncertainties. The optimisation process not only met but exceeded the reliability standards, with a significantly low probability of failure, thereby underscoring the reliability of the optimised design.

The integration of these methodologies marks a significant advancement in the field of aeroelastic design optimisation for aerospace composite structures applications. By focusing on both the optimisation of performance and the assurance of reliability, this study contributes to the development of safer, more efficient composite structures. The use of surrogate models in conjunction with probabilistic optimisation techniques represents a scalable, efficient solution to manage the complex design spaces of composite materials, manufacturing processes and operational demands.

Future Work: Looking ahead, further research could explore the integration of more complex material models and real-world operational conditions into the optimisation process. Additionally, extending this methodology to three-dimensional structures and full-scale aircraft components could provide deeper insights into the practical implications of this approach. Experimentation with alternative surrogate modeling techniques and more advanced probabilistic optimisation algorithms would also be beneficial, potentially leading to even more refined designs. Moreover, addressing the sustainability aspects of composite material usage in aerospace applications could add another dimension to this research, aligning it with the industry's increasing focus on reducing environmental impact.

In conclusion, the methods and findings of this study not only enhance our understanding of aeroelastic phenomena in composite structures but also pave the way for more innovative, efficient, and reliable aerospace design strategies in the future.

7 REFERENCES

[1] Jutte, C. and Stanford, B. (2014). Aeroelastic tailoring of transport aircraft wings: State-of-the-art and potential enabling technologies. Technical Report NASA/TM-2014-218252, NASA.

[2] Coelho, L., Lucor, D., Fabbiane, N., et al. (2023). Multi-scale approach for reliability-based design optimization with metamodel upscaling. *Structural and Multidisciplinary Optimization*, 66(205). doi:10.1007/s00158-023-03643-4.

[3] Sabater, C., Bekemeyer, P., and Görtz, S. (2020). Efficient bilevel surrogate approach for optimization under uncertainty of shock control bumps. *AIAA Journal*, 58(12).

[4] Scarth, C. and Cooper, J. E. (2018). Reliability-based aeroelastic design of composite plate wings using a stability margin. *Structural and Multidisciplinary Optimization*, 57, 1695–1709. doi:10.1007/s00158-017-1838-6. Open access.

[5] Ghiasi, H., Fayazbakhsh, K., Pasini, D., et al. (2010). Optimum stacking sequence design of composite materials part ii: Variable stiffness design. *Composite Structures*, 93(1), 1–13. ISSN 0263-8223. doi:https://doi.org/10.1016/j.compstruct.2010.06.001.

[6] Fabbiane, N., Irisarri, F.-X., Dillinger, J., et al. (2022). Aeroelastic-tailoring of a wind-tunnel model for passive alleviation of static and dynamic loads. *CEAS Aeronautical Journal*, 13(4), 967–977. doi:10.1007/s13272-022-00615-0.

[7] Weisshaar, T. (1981). Aeroelastic tailoring of forward swept composite wings. *Journal of Aircraft*, 18(8), 669–676.

[8] Jones, D. R., Schonlau, M., and Welch, W. J. (1998). Efficient global optimization of expensive black-box functions. *Journal of Global Optimization*, 13, 455–492. Printed in the Netherlands.

[9] Pelamatti, J., Brevault, L., Balesdent, M., et al. (2019). Efficient global optimization of constrained mixed variable problems. *Journal of Global Optimisation*, 73. Published online: 30 November 2018.

[10] Franco, J., Vasseur, O., Corre, B., et al. (2009). Minimum spanning tree: A new approach to assess the quality of the design of computer experiments. *Chemometrics and Intelligent Laboratory Systems*, 97(2), 164–169.

[11] Chen, V., Tsui, K., Barton, R., et al. (2003). A review of design and modeling in computer experiments. *Handbook of Statistics*, 22, 231–261.

[12] Li, X., Yang, Q., Wang, Y., et al. (2021). Development of surrogate models in reliability-based design optimization: A review. *Mathematical Biosciences and Engineering*, 18(5), 6386–6409. doi:10.3934/mbe.2021317.

[13] Dubourg, V., Sudret, B., and Bourinet, J.-M. (2011). Reliability-based design optimization using kriging surrogates and subset simulation. *Structural Multidisciplinary Optimization*. doi:10.1007/s00158-011-0653-8.

[14] Saves, P., Lafage, R., Bartoli, N., et al. (2024). SMT 2.0: A surrogate modeling toolbox with a focus on hierarchical and mixed variables gaussian processes. *Advances in Engineering Sofware*, 188, 103571. doi:https://doi.org/10.1016/j.advengsoft.2023.103571.

[15] Irisarri, F.-X., Lasseigne, A., Leroy, F.-H., et al. (2014). Optimal design of laminated composite structures with ply drops using stacking sequence tables. *Composite Structures*, 107, 559–569.

[16] Soremekun, G., Gürdal, Z., Kassapoglou, C., et al. (2002). Stacking sequence blending of multiple composite laminates using genetic algorithms. *Composite Structures*, 56(1), 53–62.

[17] Kameyama, M. and Fukunaga, H. (2007). Optimum design of composite plate wings for aeroelastic characteristics using lamination parameters. *Computers & Structures*, 85(3-4), 213–224.

[18] Kim, T.-U. and Hwang, I. H. (2005). Optimal design of composite wing subjected to gust loads. *Computers & Structures*, 83(19-20), 1546–1554.

[19] Bailie, J. A., Ley, R. P., and Pasricha, A. (1997). Summary and review of composite laminate design guidelines. Tech. rep., Northrop Grumman Corporation, Military Aircraft Systems Division. NASA Contract NAS1-19347, Final Report June 1997 – October 1997.

[20] Tsai, S. W., Halpin, J. C., and Pagano, N. J. (1968). *Composite Materials Workshop*. Stamford, CT: Technomic Pub. Co.

[21] Hassig, H. J. (1971). An approximative true damping solution of the flutter equation by determinant iteration. *Journal of Aircraft*, 8(11), 885–889.

[22] Baker, M. L., Mendoza, R., and Hartwich, P. M. (1999). Transonic aeroelastic analysis of a high speed transport wind tunnel model. In *Proceedings of the AIAA Conference*, AIAA-99-1217. pp. 1999–1217.

[23] Riso, C. and Cesnik, C. E. S. (2022). Investigation of geometrically nonlinear effects in the aeroelastic behavior of a very flexible wing. In *2023 AIAA SciTech Forum*. National Harbor, MD and Online, pp. –. doi:10.2514/6.2023-0759.

[24] An, H., Youn, B. D., and Kim, H. S. (2021). Reliability-based design optimization of laminated composite structures under delamination and material property uncertainties. *International Journal of Mechanical Sciences*, 205, 106561.

COPYRIGHT STATEMENT